JOURNAL OF MATERIALS SCIENCE **39** (2004) 2365–2370

Synthesis of nanocrystalline magnetite by mechanical alloying of iron and hematite

M. D. ALCALÁ, J. M. CRIADO, C. REAL
Institute of Material Sciences, University of Sevilla C.S.I.C., c/Américo Vespucio s/n, 41092 Sevilla, Spain
E-mail: mdalcala@cus.es

T. GRYGAR, M. NEJEZCHLEBA, J. SUBRT
Institute of Inorganic Chemistry ASCR, Rez uPrahy, Czech Republic

E. PETROVSKY
Geophysical Institute ASCR, Bocní ll/1401, 141 31 Prague 4, Czech Republic

The synthesis of magnetite has been studied by mechanical alloying in an inert atmosphere of a stoichiometric mixture of micrometric particle size iron and hematite powders. The final products have been characterised by chemical analysis, SEM, TEM, XRD, Mössbauer spectroscopy as well as specific surface and magnetic measurements. The magnetite obtained in this way exhibits a high magnetic hardness. The formation of a wüstite layer on the magnetite core, because of the reaction between magnetite and iron contamination coming from the bowls and grinding balls, tends to decrease the coercive force of magnetite. The formation of this phase would be avoided by controlling the grinding time.

1. Introduction

Synthetic magnetite has been extensively used in different industrial processes [1]. Magnetite is one of the major synthetic iron oxide pigments and it has been used to produce printing colours and the magnetic inks used in photocopying and facsimile machines. It's low cost, high stability, chemical properties and capability to withstand a high level of impurities without being poisoned make it one of the principal iron oxides used in catalysis of industrial reactions. Owing to their hardness, magnetite has been used as abrasives and polishing agents. Magnetite has been also used as the dense medium in mineral separation processes. This material is used as precursor of maghemite, a magnetic compound of great technological importance in ferrofluids, and as raw material for manufacturing catalyst and magnetic recording supports [2–4]. Recently, there has been considerable interest in magneto-optic devices that combine magnetic and optical phenomena [5]. This application demands iron oxide with particle sizes lower than 10 nm. On the other hand, magnetic nanostructured materials are characterised by new and unexpected magnetic properties [6, 7], such as an unusual increment of the remanence or coercivity.

Because of their importance in magnetic materials technology, preparation and properties of iron oxides have been the subject of numerous studies [5, 8–21]. Many of these studies have used mechanical attrition to obtain different iron systems [9–14]. Mechanical attrition has attracted increasing interest in recent years [22] to make nanocrystalline, amorphous and metastable materials because of its simplicity, the relatively inexpensive equipment needed and the applicability to essentially all classes of materials [23–28]. Nanostructured materials are characterised by structural domain size of the order of a few nanometers in at least one dimension and for at least one component of the sample. These materials have a significant atom fraction associated with interfacial environments. As a result, their properties can be different from and often superior to, those of conventional materials with phase or grain structures on a coarser size scale [6]. In the case of iron systems, high-energy ball milling has been recently used for the production of Fe_3O_4/Fe magnetic nanocomposites with high values of coercivity [10, 14].

The scope of this work is to study the mechanical attrition of a stoichiometric mixture of hematite and iron under inert atmosphere. The results of the milled powder characterisation have also been reported. Their magnetic properties were studied in a previews paper [19].

2. Experimental

Metallic iron (<10 μm, 99.9+ %) and hematite (1 μm, 99+ %) powders supplied by Aldrich® have been used as starting materials. Samples of 5 g were prepared by mixing iron and hematite powders according to the stoichiometric proportions of the following reaction:

$$4Fe_2O_3 + Fe \rightarrow 3Fe_3O_4 \quad (1)$$

The milling process was carried out in a high-energy planetary ball mill Fritsch®, model Pulverissette 7, equipped with steel vials with 45 cc capacity containing 7 steel balls, 15 mm in diameter. The mill is equipped with a rotating valve that allows it to operate in permanent connection to a gas cylinder. A pressure transducer attached to the valve permits work at any constant pressure selected by the user in the range from 1 to 10 bar. Two funnels close to the grinding vials were used for cooling the sample all over the grinding process. A steady-temperature lower than 50°C was reached after about 30 min of grinding and was maintained for higher grinding times.

The samples were ground under nitrogen atmosphere in order to avoid oxidation. For this purpose, the air initially contained in the grinding jar was outgassed before filling with nitrogen. The nitrogen pressure was maintained at a constant value of 2 bars in order to prevent the entrance of gas from the atmosphere. A rotation speed equal to 830 r.p.m. and a ball to powder weight ratio close to 18 were used. The iron-hematite mixture samples were ground under these conditions from 30 min to almost 5 h. The sample description and labelling is summarised in Table I.

X-ray diffraction (XRD) analysis of the milled samples was performed with a Siemens D-501 diffractometer, equipped with a graphite monochromator and a fixed slit, using Cu K_α radiation. The size of the coherently diffracting domains (D) of the hematite and magnetite particles has been determined from the analysis of the (104) and (220) profiles, respectively. X-ray methods are statistically justified as XRD peaks average diffraction effects from a large number of individual size particles [29]. Two different methods have been used, i.e., Scherrer [30] and the variance [31]. Scherrer method gives maximum crystallite size values. The variance procedure allows the simultaneous determination of both the crystallite size (D) and the root-mean square ($\langle\varepsilon^2\rangle^{1/2}$) of the microstrains. It is well known that "D" values given by this last method are lower than the ones calculated from Scherrer method although they follow the same trend.

^{57}Fe Mössbauer spectra were recorded at room temperature in transmission geometry by using a source of ^{59}Co in a Cr matrix moving in constant acceleration regime. Isomer shifts were referred to α-Fe. During the fitting procedure of the spectra the following quantities were left free: the line widths and their distributions, quadrupole splitting, isomer shift and hyperfine field.

TABLE I Sample description and labelling

Sample label	Sample description
M0-00	Starting mixture of iron and hematite raw materials according to the stoichiometric proportion given by Equation 1.
M0-32	Magnetic powder produced by ball milling of sample M0-00 during 32 min (nitrogen atmosphere at a pressure of 2 bar)
M1-10	Same as M0-32, milling time 1 h 10 min
M1-47	Same as M0-32, milling time 1 h 47 min
M3-09	Same as M0-32, milling time 3 h 09 min
M4-50	Same as M0-32, milling time 4 h 50 min

The specific surface area was measured by the BET method using a Adsorptmeter Micromeritics, model 2200. The apparent equivalent diameter of the particles can be estimated by assuming spherical symmetry according to the following expression:

$$d_{\mathrm{BET}} = \frac{6}{\rho S} 10^3 \qquad (2)$$

d_{BET} being the diameter of the particle in nanometers; ρ is the density of the solid expressed in g/cm^3 ($\rho' = 5.20$ g/cm^3 for magnetite) and S represent the specific surface given in m^2/g.

Scanning (SEM) and transmission (TEM) electron microscopy were carried out in a Philips XL30 microscope and in a Philips CM200 microscope, respectively.

The Fe(II)/Fe(total) ratio in the milled samples was determined by dissolving the sample in a diluted mixture of H_3PO_4 and H_2SO_4 under nitrogen atmosphere. Fe(0) is dissolved like Fe(II) while Fe(II) and Fe(III), initially present in the solid sample, preserve their oxidation states under these experimental conditions. The resulting Fe(II) was determined by titration with $KMnO_4$ solution. The total iron was determined after dissolution of the sample in dilute HCl by chelatometric titration. Thus, the Fe(II) figure determined from the chemical analysis is accounting for the total amount of Fe(II) + Fe(0).

The abrasive stripping voltammetry has been used in addition for checking the presence of Fe(0) in the cases that metallic iron was not detected by XRD. For this purpose, samples were mechanically deposited on the working electrode, a paraffin impregnated spectral graphite rod. The electrode was used for voltammetry in three-electrode measuring system with platinum plate as counter electrode and saturated calomel reference electrode. The solution of 0.5 M $NaClO_4$ and 0.1 M $HClO_4$ was used as supporting electrolyte. The voltammograms were obtained by scanning from open circuit potential towards negative potentials. The reductive dissolution of iron oxides yielded well defined cathodic peaks as described elsewhere [32–34]. In the presence of metallic iron sharp anodic peaks were superimposed on the cathodic peaks.

Magnetic measurements were made using a KLY-3 Kappabridge for the temperature dependence of magnetic susceptibility and a Princeton Vibrating Sample Magnetometer (MicroMag™, Model 3900 VSM) for the hysteresis loops.

3. Results and discussion

Fig. 1 shows the evolution of the X-ray diffractograms for the Fe/α-Fe_2O_3 mixed samples during ball milling. An important reduction of the hematite crystal size is already observed in the sample M0-32 as shown by the broadening of the corresponding X-ray lines. Further milling still promotes this crystal size refinement at the

TABLE II Particle and crystal sizes of the starting raw material and ground samples

	Hematite phase			Magnetite phase				
Sample	D_{104}(nm) (Scherrer)	D_{104}(nm) (Variance)	$\langle E^2\rangle^{1/2}$	D_{220}(nm) (Scherrer)	D_{220}(nm) (Variance)	$\langle E^2\rangle^{1/2}$	S_{BET} (m^2/g)	d_{BET} (μm)
M0-00	589	245	1.29×10^{-3}	–	–	–	–	–
M0-32	129	45	4.10×10^{-3}	–	–	–	–	–
M1-10	113	40	4.56×10^{-3}	65	–	–	–	–
M1-47	118	43	4.25×10^{-3}	77	25	7.36×10^{-3}	–	–
M3-09	–	–	–	90	31	6.29×10^{-3}	<1	1.2
M4-50	–	–	–	86	27	6.91×10^{-3}	3	0.4

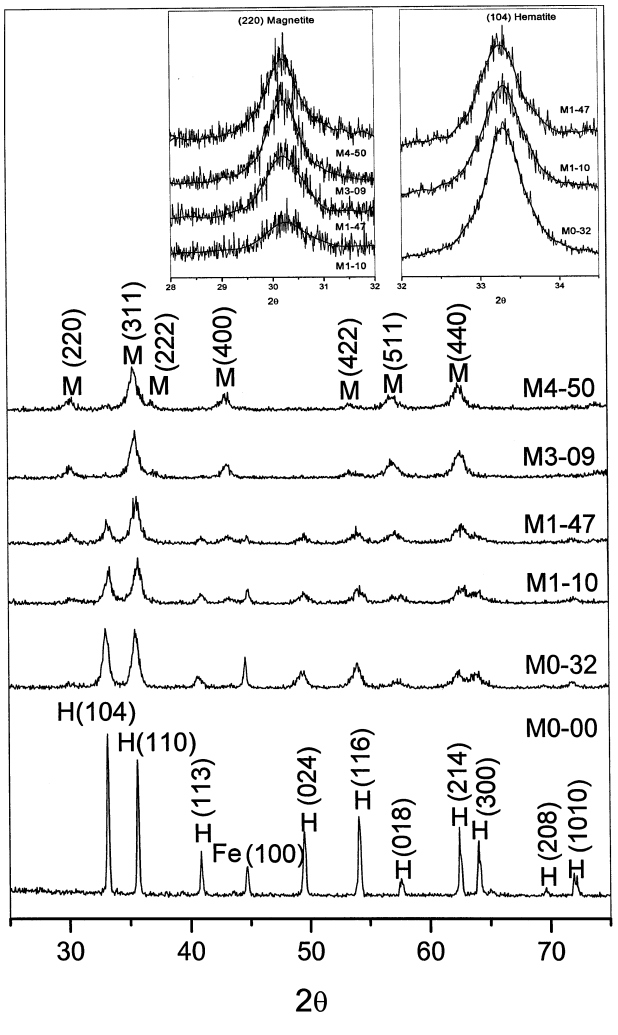

Figure 1 XRD diffraction diagrams of the ground samples.

time that produces the transformation of this phase into magnetite. After 3 h 9 min milling (M3-9 sample) the reaction (1) is nearly completed and the diffractogram indicates that magnetite is the only phase present in this sample. It is well known that XRD patterns of Fe_3O_4 and γ-Fe_2O_3 are very similar and it is difficult to distinguish between the two phases. However, the formation of maghemite is not expected if we consider both that the Fe_3O_4 cannot be oxidized because we are working under a high pressure of pure nitrogen and that the transformation of hematite to maghemite by ball mill dry grinding does not take place [35, 36]. Further milling does not seem to produce any change in the composition and microstructure of the final product. Table II shows the average crystal sizes of hematite and magnetite phases determined from the X-ray analysis for the set of samples here prepared. The results included in Table II show that the average size of the hematite nanocrystals reported for the sample M0-32 only changes slightly by increasing the grinding time. Moreover, the reaction between iron and the hematite nanocrystals promotes the formation of nanocrystals of magnetite with an average crystal size smaller than that of the precursor hematite. The microstrain data of the hematite and magnetite phases, also included in Table II, point out an inverse relationship between the crystal size and the microstrains level. A similar relationship has been found for other materials subjected to thermal or mechanical treatment [37]. This behaviour could be explained [38] by assuming that the particles are formed by small crystallites welded in a mosaic structure and that the grain boundaries constitute the main contribution to the microstrains. This assumption is supported by the study of the SEM micrographs reported for the samples M3-09 (Fig. 2a) and M4-50 (Fig. 2b). It can be observed that the particle sizes outlined from this figure are in the microns region and, therefore, these sizes are considerably higher than the corresponding sizes of the diffraction microdomains reported in Table II. The TEM micrograph of sample M3-09 (Fig. 2c) shows that the average size of the crystals in the aggregates is in the range calculated from the XRD data. On the other hand, the comparison of Fig. 2a and b suggests that the sample M3-09 has a larger aggregate size than the sample M4-50. This fact is in agreement with the data of specific area determined for these samples and the corresponding particle sizes estimated from Equation 1 included in Table II.

Mössbauer spectroscopy allows achieving a more exhaustive study of the composition of the milled samples than X-ray diffraction. At room temperature and in a zero external magnetic field, the Mössbauer spectra (MS) of magnetite and maghemite are different: the Mössbauer spectrum of γ-Fe_2O_3 can be interpreted as a unique sextet, whereas the Mössbauer spectrum of magnetite is commonly interpreted as a superposition of two sextets [21]. Recorded MS have been included in Fig. 3a. These spectra were fitted by computing several sextets in addition to a doublet generally attributable to the different phases that could be present in the sample. Fig. 3b shows the phase analysis extracted from

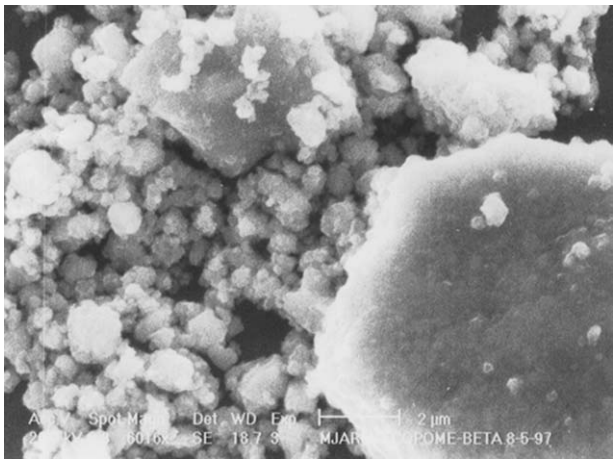

(a)

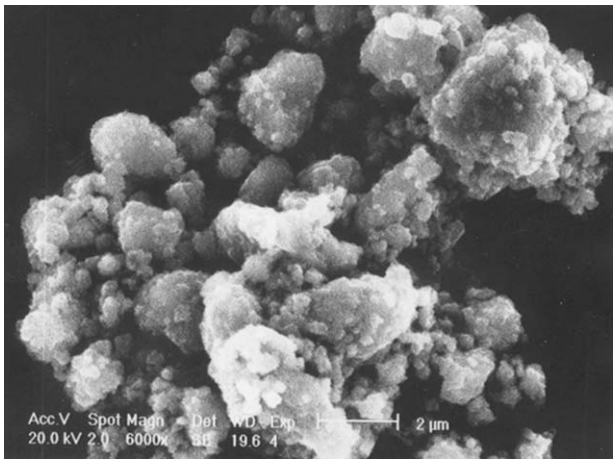

(b)

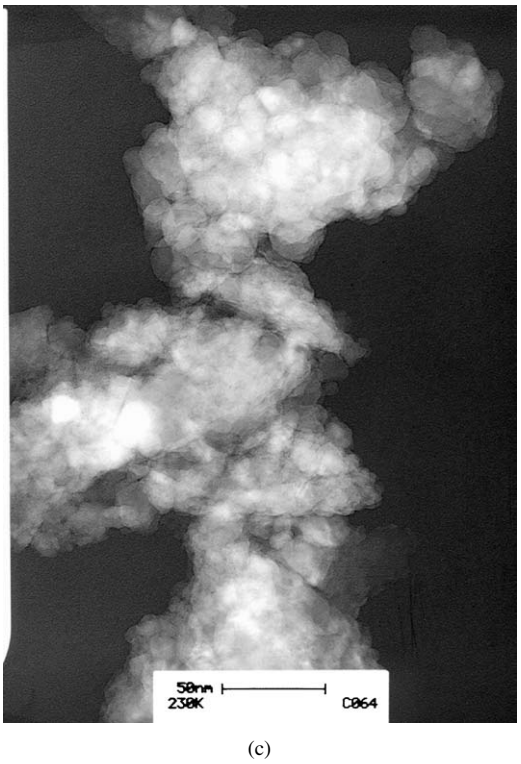

(c)

Figure 2 (a), (b) SEM micrographs of samples M3-09 and M4-50, respectively and (c) TEM micrograph of sample M3-09.

the MS. The results included in Fig. 3 point out that the reaction (1) is in progress in the sample M0-32, provided that its corresponding spectrum clearly shows the presence of magnetite besides the metallic iron and hematite used as raw materials. It is observed that the area percentages of the iron and hematite Mössbauer peaks decrease by increasing the grinding time and at the time that the total contribution of the peaks assigned to magnetite increases. Moreover, Fig. 3b shows that neither hematite nor metallic iron were found in the sample M3-09 what indicates that a full conversion has been already reached. Thus, the percentage of the reactants remains equal to zero if the grinding continues in progress. The analysis of the MS of the samples M3-09 and M4-50 point out that non-stoichiometric magnetite has been obtained. In these samples, the peaks corresponding to Fe^{2+} and Fe^{3+} in octahedral coordination (B sites) are so broad that they cannot be fitted just with one sextet. Thus, two sextets have been required for a proper fitting of these broad Mössbauer peaks. This broadening perhaps would be explained by considering that a large amount of lattice defects are generated during the grinding process.

On the other hand, it is noteworthy to remark that a doublet assigned to paramagnetic iron emerges in the Mössbauer spectrum of the sample M1-10 and the contribution of this phase to the composition of the sample increases by increasing the milling time until reaching a value close to 11% in the sample M4-50. The XRD and Mössbauer data previously reported are not enough for discerning the paramagnetic phase leading to the MS doublet. Additional information would be required for phase assignation of this doublet as it will be discussed below.

The $(Fe(0) + Fe^{2+})$/Fe (total) ratios determined from the chemical analysis of the samples are shown in Table III together with their corresponding conversion percentages calculated by bearing in mind that the starting sample is constituted by a mixture of iron and hematite according to the stoichiometric proportion given by Equation 1. The magnetite conversions estimated from the percentage of hematite remaining in the Mössbauer spectra of the ground samples are also included in Table III. These values show a good agreement with those obtained from the chemical analysis,

TABLE III Phase composition and coercive field (H_c) of magnetite obtained by mechanical alloying

Sample	$\frac{(Fe(0) + Fe(II))}{Fe(total)}$	[a]Conversion (c.a.) (%)	[b]Conversion (MS) (%)	H_c (mT)
M0-32	0.26	67	50	19.4
M1-10	0.23	53	57	26.7
M1-47	0.29	80	83	31.9
M3-09	0.33	100	100	36.1
M4-50	0.40	Full conversion + Fe(II) excess	100	35.0

[a]Calculated from the ratio $(Fe(0) + Fe(II))$/Fe (total) determined by chemical analysis (c.a.).
[b]Determined from the hematite conversion as determined from Mössbauer spectroscopy (MS).

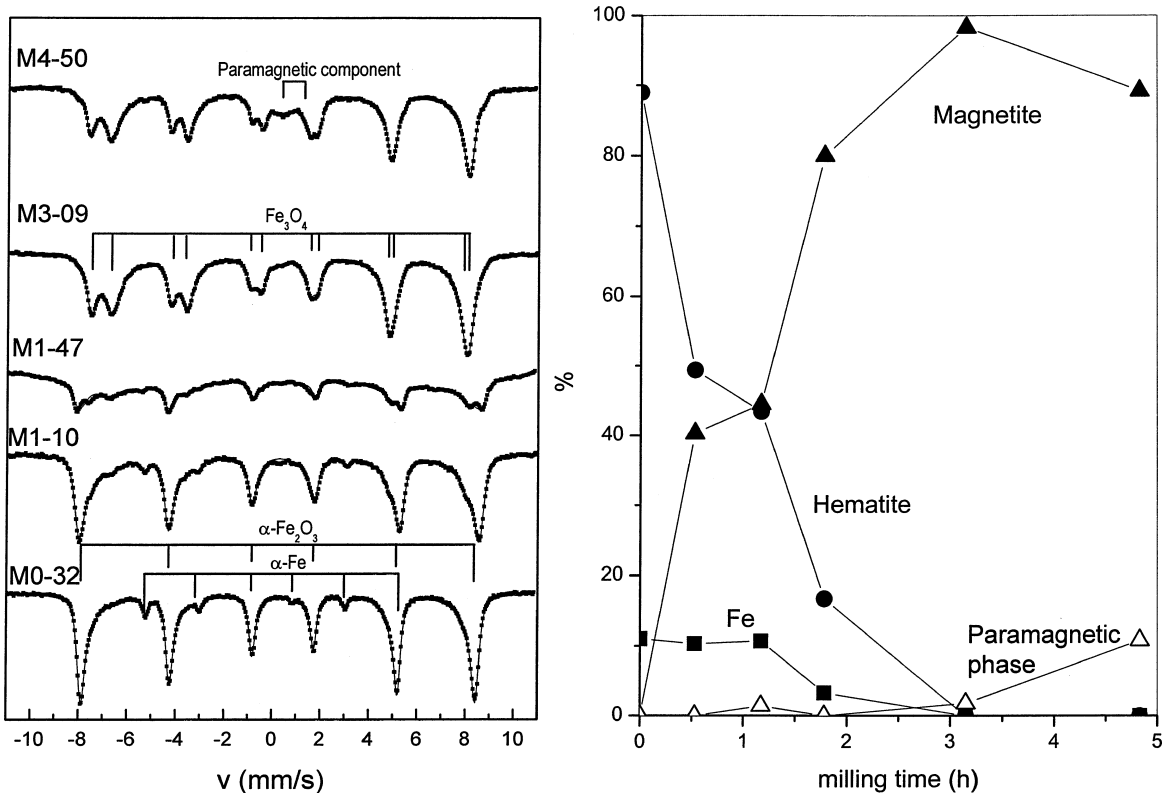

Figure 3 (a) Mössbauer spectra of the ground samples and (b) phase analysis (% = %Fe calculated on all Fe as relative spectral area).

with the only exception of the M0-32 sample. This behaviour could be explained by considering that the first sample ground was the M0-32 sample. At the beginning of the experiment the surfaces of both the grinding balls and the bowl walls were not still covered by a protective layer of the ground material, this fact would lead to an excess of iron because of a relative higher contamination from the grinding media. It must be pointed out that Fe(0) has not been found from the abrasive stripping voltametry analysis of the samples M3-09 and M4-50 in agreement with the Mössbauer analysis results. Thus, the large excess of iron reported for the sample M4-50 would be as Fe(II). It is well known [1] that the total amount of Fe(II) present in the magnetite lattice is filling half of the octahedral sites (B sites). Provided that all these positions of the spinel lattice are occupied, an excess of Fe(II) cannot be accepted without disrupting the structure of magnetite. Cornell and Schwertmann have shown in a recent revision [1] that magnetite with an excess of Fe(II) has never been reported in literature while non-stoichiometric Fe(II) defective magnetite exhibiting an Fe(II)/Fe(total) ratio lower than the value of 0.33, expected for a stoichiometric magnetite, are very common. Thus, the excess of Fe(II) here reported could be assigned to the formation of FeO (wüstite). A finely divided wüstite phase that cannot be detected by XRD could account for the paramagnetic component observed in the MS that reach a value of 10.8% in the sample M4-50.

The above results allow us to propose that besides the conversion of hematite and iron into magnetite according Equation 1, a lateral reaction between the magnetite and the iron contamination coming from the bowl and balls seems to take place leading to the formation of wüstite according to the following equation:

$$Fe_3O_4 + Fe \rightarrow 4FeO \quad (3)$$

The synthesis of FeO by mechanical alloying according to Equation 3 has been previously reported in the literature [10, 13].

It is noteworthy to remark that the magnetic hardness of the magnetite obtained for the ground samples is considerably higher than that expected for single-domain (SD) magnetite [19]. The milled samples exhibit coercive field, H_c, of 19 to 36 mT as shown in Table III. For comparison, the commonly accepted value for SD magnetite is 10 mT [39]. The results included in Table III point out that the coercive field H_c increases by increasing the grinding time when we move from the sample M0-32 to the M3-09 one. However, the sample M4-50 undergoes a diminution of H_c with regard to the sample M3-09. The diminution of H_c seems to be associated to the important increase of the contribution of the paramagnetic phase, here ascribed to the formation of wüstite, to the overall phase composition of the M4-50 sample as reported in Fig. 3b. The enhanced magnetic hardness could be explained on the basis of the nanostructure nature of the obtained powder and by the presence of a surface layer with high concentration of defects induced by the milling process.

4. Conclusions

Nanostructure magnetite with a high magnetic hardness has been synthesized by mechanical alloying in an inert atmosphere. The obtained samples exhibit coercive magnetic force three times higher than that typical

for single domain natural magnetite. The X-ray and Mössbauer data suggest that the M4-50 sample is constituted by a combination of non-oxidised magnetite core with a highly wüstitised surface. The formation of wüstite seems to reduce the coercive field of magnetite, but its formation would be avoided by controlling the grinding time.

References

1. R. M. CORNELL and U. SCHWERTMANN,"The Iron Oxides," edited by VCH (Germany, 1996).
2. K. RAJ and R. MOSKOVITZ, *J. Magn. Magn. Mater.* **85** (1990) 223.
3. C. SESTIER, M. F. DASILVA, D. SABOLOVIA, J. ROGER and J. N. PONS, *Electrophoresis* **19** (1998) 1220.
4. F. GAZOEAU, J. C. BACRI, F. GENDRON, R. PERZYNSKY, Y. L. RAIKHER, V. I. STEPANOV and E. DUBOIS, *J. Magn. Magn. Mater.* **186** (1998) 157.
5. Y. S. KANG, S. RISBUD, J. F. RABOLT and P. STROEVE, *Chem. Mater.* **8** (1996) 2209.
6. H. GLEITER, *Progr. Mater. Sci.* **33** (1989) 223.
7. M. SOLZI, "Fundamental Properties of Nanostructured Materials," edited by D. Fiorani and G. Sberveglieri (London, 1993).
8. M. P. MORALES, C. PECHARROMAN, T. GONZÁLEZ CARREÑO and C. J. SERNA, *J. Solid State Chem.* **108** (1994) 158.
9. J. Z. JIANG, Y. X. ZHOU, S. MØRUP and C. BENDER KOCH, *NanoStruct. Mater.* **7**(4) (1996) 401.
10. J. DING, W. F. MIAO, R. STREET and P. G. McCORMICK, *Scripta Materialia* **35**(11) (1996) 1307.
11. S. LINDEROTH, J. Z. JIANG and S. MØRUP, *Mater. Sci. Forum* **235–238** (1997) 205.
12. E. HERRERO, M. V. CABAÑAS, M. VALLET-REGÍ, J. L. MARTÍNEZ and J. M. GONZÁLEZ-CALBET, *Solid State Ion.* **101–103** (1997) 213.
13. G. F. GOYA, H. R. RECHENBERG and J. Z. JIANG, *J. Appl. Phys.* **84**(2) (1998) 1101.
14. J. DING, W. F. MIAO, E. PIRAULT, R. STREET and P. G. McCORMICK, *J. Magn. Magn. Mater.* **177–181** (1998) 933.
15. V. ŠEPELÁK, S. WIßMANN and K. D. BECKER, *ibid.* **203** (1999) 135.
16. M. BLANCO-MANTECÓN and K. O'GRADY, *ibid.* **203** (1999) 50.
17. T. TOYODA, S. SASAKI and M. TANAKA, *Amer. Mineral.* **84** (1999) 294.
18. G. S. CHOPRA, C. REAL, M. D. ALCALÁ, L. A. PÉREZ-MAQUEDA, J. ŠUBRT and J. M. CRIADO, *Chem. Mater.* **11** (1999) 1128.
19. E. PETROVSKÝ, M. D. ALCALÁ, J. M. CRIADO, T. GRYGAR, A. KAPICKA and J. ŠUBRT, *J. Magn. Magn. Mater.* **210** (2000) 257.
20. Y. NI, X. GE, Z. ZHANG and Q. YE, *Chem. Mater.* **14** (2002) 1048.
21. R. ZBORIL, M. MASHLAN and D. PETRIDIS, *ibid.* **14** (2002) 969.
22. C. C. KOCH, *NanoStruct. Mater.* **9** (1997) 13.
23. G. J. FAN, F. Q. GUO, Z. Q. HU, M. X. QUAN and K. LU, *Phys. Rev.* B **55**(17) (1997) 11010.
24. H. ZHANG and E. H. KISI, *J. Alloys Comp.* **248** (1997) 201.
25. T. KLASSEN, M. OEHRING and R. BORMANN, *Acta Mater.* **45**(9) (1997) 3935.
26. K. J. BRYDEN and J. Y. YING, *ibid.* **44**(9) (1996) 3847.
27. P. MATTEAZZI and M. D. ALCALA, *Mater. Sci. Eng.* A **230** (1997) 161.
28. R. S. FIGUEIREDO, A. MESSAI, A. C. HERNANDES and A. S. B. SOMBRA, *J. Mater. Sci. Lett.* **17**(6) (1998) 449.
29. A. WIEWIÓRA, J. L. PÉREZ-RODRÍGUEZ, L. A. PÉREZ-MAQUEDA, J. DRAPALA and M. KUZNIARSKI, subbitted to *J. Appl. Clay Sci.* (2002).
30. H. P. KLUNG and E. ALEXANDER, "X-Ray Diffraction Procedures for Polycrystalline and Amorphous Materials" (John Wiley, New York, 1974).
31. H. J. EDWARDS and K. TOMAN, *J. Appl. Cryst.* **2** (1964) 240.
32. F. SCHOLZ and B. MEYER, in "Electroanalytical Chemistry," A Series of Advances, edited by A. J. Bard and I. Rubinstein (Marcel Dekker, Inc, 1998) Vol. 20, p. 1.
33. T. GRYGAR, *J. Electroanal. Chem.* **405** (1996) 117.
34. T. GRYGAR, P. BEZDICKA and E.-G. CASPARY, *ibid.* **146** (1999) 3234.
35. E. MENDELOVICI, S. NEDIV and I. LIN, *J. Mater. Sci.* **19** (1983) 1556.
36. R. GÓMEZ-VILLACIEGOS, L. HERNÁN, J. MORALES and J. L. TIRADO, *Mater. Res. Bull.* **22** (1987) 513.
37. J. M. CRIADO, M. GONZÁLEZ and C. REAL, *J. Mater. Sci. Lett.* **5** (1986) 467.
38. J. M. CRIADO and C. REAL, *Mater. Sci. Monogr.* **288** (1985) 749.
39. R. THOMPSON and F. OLDFIELD, "Environmental Magnetism" (Allen and Unwin, London, 1986).

Received 28 May
and accepted 13 November 2003